Predictive Analytical and Thermal Modeling of Orthogonal Cutting Process—Part I: Predictions of Tool Forces, Stresses, and Temperature Distributions

Yiğit Karpat

Tuğrul Özel[1]
e-mail: ozel@rci.rutgers.edu

Department of Industrial and Systems Engineering,
Rutgers University,
Piscataway, NJ 08854

In this paper, a predictive thermal and analytical modeling approach for orthogonal cutting process is introduced to conveniently calculate forces, stress, and temperature distributions. The modeling approach is based on the work material constitutive model, which depends on strain, strain rate, and temperature. In thermal modeling, oblique moving band heat source theory is utilized and analytically combined with modified Oxley's parallel shear zone theory. Normal stress distribution on the tool rake face is modeled as nonuniform with a power-law relationship. Hence, nonuniform heat intensity at the tool-chip interface is obtained from the predicted stress distributions utilizing slip line field analysis of the modified secondary shear zone. Heat sources from shearing in the primary zone and friction at the tool-chip interface are combined, heat partition ratios are determined for temperature equilibrium to obtain temperature distributions depending on cutting conditions. Model validation is performed by comparing some experimental results with the predictions for machining of AISI 1045 steel, AL 6082-T6, and AL 6061-T6 aluminum. Close agreements with the experiments are observed. A set of detailed, analytically computed stress and temperature distributions is presented.
[DOI: 10.1115/1.2162590]

Keywords: heat source method, heat partition, non-uniform heat intensity, tool forces, tool stresses, temperature distributions

1 Introduction

Modeling metal cutting processes with the aid of plasticity theory has been of great interest to researchers. Mainly, two fundamental approaches have been extensively researched: (1) the minimum energy principle [1–3] and (2) the slip line field theory [2,4]. The most significant contribution to the field is the parallel-sided shear zone theory introduced by Oxley [4] to predict cutting forces and machining variables in orthogonal cutting by constructing slip line fields around the primary shear zone. Oxley's machining theory uses the dependence of material flow upon strain, strain rate, and temperature to obtain the shear angle and other outputs of interest by considering the workpiece material properties, tool geometry, and cutting conditions [5,6]. Cutting forces, stresses, and temperatures in the deformation zones and on the tool faces are important to model properly tool wear mechanisms and the properties of the finished surface. In an earlier work, Özel and Zeren [7] presented modifications to Oxley's analysis of machining and proposed a methodology to determine work material flow stress based on the Johnson-Cook (JC) constitutive model [8] and friction characteristics at the tool-chip interface by using orthogonal cutting tests. The objective of this study is to obtain cutting forces, stress distributions on the tool rake face, and temperature distributions in the deformation zones. This will be achieved by modeling heat intensity at the secondary shear zone as nonuniform by utilizing the modifications to Oxley's theory proposed by Özel and Zeren [7] where the secondary deformation zone was modeled as triangular in shape. This approach will enable us to obtain normal and frictional shear stress distributions and lengths of sticking and sliding zones along the tool-chip interface, which will be utilized later to model nonuniform heat intensity as the heat source in the secondary shear zone.

Modeling machining temperatures has attracted many researchers due to the complexity of measuring temperatures during machining. Many analytical models have been proposed to predict temperature distributions in the deformation zones. Pioneering studies were performed by Hahn [9], Trigger and Chao [10], Chao and Trigger [11], Loewen and Shaw [12], Leone [13], Boothroyd [14] and recently by Komanduri and Hou [15–17] and Huang and Liang [18].

1.1 Constitutive Models for Work Material Flow Stress. This study considers Johnson-Cook work material models for AISI 1045 steel, AL 6082-T6 aluminum, and AL 6061-T6 aluminum as adapted from Jaspers and Dautzenberg [19], Adibi-Sedeh et al. [20] and Johnson et al. [21] respectively. The JC work material model describes the flow stress of the material by considering strain, strain rate, and temperature effects as given in Eq. (1).

$$\bar{\sigma} = [A + B(\bar{\varepsilon})^n]\left[1 + C\ln\left(\frac{\dot{\bar{\varepsilon}}}{\dot{\bar{\varepsilon}}_0}\right)\right]\left[1 - \left(\frac{T - T_0}{T_m - T_0}\right)^m\right] \quad (1)$$

The constants A, B, C, n, and m of the model are obtained by Split Hopkinson Pressure Bar (SHPB) tests conducted at strain ranges of 0.05 to 0.2, strain-rate of 7500 1/s, and temperature ranges of 35°C to 625°C by Jaspers and Dautzenberg [19] for AISI 1045 steel and AL 6082-T6 aluminum alloy as modified by Adibi-Sedeh et al. [20] as given in Table 1.

[1]To whom correspondence should be addressed.

Contributed by the Manufacturing Engineering Division of ASME for publication in the JOURNAL OF MANUFACTURING SCIENCE AND ENGINEERING. Manuscript received May 19, 2005; final manuscript received September 16, 2005. Review conducted by W. J. Endres.

Table 1 Johnson-Cook material constants obtained from SHPB tests

Material	T_m (°C)	A (MPa)	B (MPa)	C	n	m
AISI 1045 [26]	1460	553.1	600.8	0.0134	0.234	1
AL 6061-T6 [21]	582	324	114	0.002	0.42	1.34
AL 6082-T6 [20]	582	250	243.6	0.00747	0.17	1.31

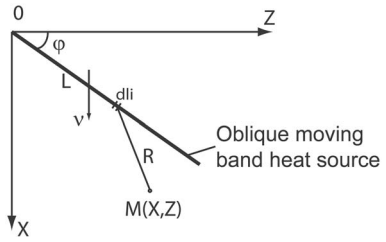

Fig. 1 Oblique moving band heat source in an infinite medium

2 Thermal Modeling of the Cutting Process

Temperature modeling of metal cutting is highly important since it directly affects the process variables such as the cutting forces and the contact length both of which are required to model wear mechanisms. The analytical modeling of steady state temperature in metal cutting presented by Hahn [9] is based on the heat source method of Jaeger [22]. As shown in Fig. 1, the temperature rise T_M under the effect of the oblique moving band uniform heat source with a velocity ν can be expressed as in Komanduri and Hou [15].

$$T_M(X,Z) = \frac{q}{2\pi\lambda_i}\int_{l_i=0}^{L} e^{-(X-l_i\sin\varphi)(\nu/2a_i)} \times K_0\left[\frac{\nu}{2a_i}\sqrt{(X-l_i\sin\varphi)^2+(Z-l_i\cos\varphi)^2}\right]dl_i \quad (2)$$

Komanduri and Hou [16] modified the coordinate system of Hahn's solution for an oblique band heat source in an infinite medium to simplify the derivation of equations for shear plane heat source (q_{shear}) which is moving in a semi-infinite medium where the work surface and the chip surface are the boundaries of a semi-infinite medium. However, since those boundaries were not considered in Hahn's solution, an appropriate image heat source is added to the model as shown in Fig. 2.

The temperature rise at any point $M(X,Z)$ caused by the moving line heat source is due to the combined effect of the primary and image heat sources and can be calculated using Eq. (3).

$$T_{M_{\text{shear}}}(X,Z) = \frac{q_{\text{shear}}}{2\pi\lambda_c}\int_{l_i=0}^{l_{AB}} e^{-(X-l_i\sin\phi)(V_c/2a_c)} \times\left\{K_0\left[\frac{V_c}{2a_c}\sqrt{(X-l_i\sin\phi)^2+(Z-l_i\cos\phi)^2}\right] + K_0\left[\frac{V_c}{2a_c}\sqrt{(X-l_i\sin\phi)^2+(Z+l_i\cos\phi)^2}\right]\right\}dl_i \quad (3)$$

Heat intensity at primary shear zone due to shearing can be modeled uniformly as

$$q_{\text{shear}} = \frac{F_s V_s}{l_{AB} w} \quad (4)$$

Komanduri and Hou [16] proposed that oblique band heat source moving at chip velocity V_c can be used to model temperature rise at any point on the chip, and oblique band heat source moving at cutting velocity V can be used to model temperature rise at any point in the workpiece due to primary heat source. In this study, it is assumed that all of the deformation energy caused by shearing in primary shear zone is converted into heat.

The effect of secondary heat source is modeled by considering tool-chip interaction. Chao and Trigger [11] assumed uniform heat intensity with nonuniform heat partition ratio at the tool-chip interface, and they used the functional analysis method to find a temperature distribution along the tool-chip interface. Komanduri and Hou [16] extended the functional analysis based on the work of Chao and Trigger. However, because of the presence of plastic and elastic zones along contact length, secondary heat source cannot be assumed as uniform. Recently, Huang and Liang [18] used the nonuniform heat intensity along tool-chip interface in their model by converting uniform shear stress distribution to an assumed shear stress distribution without calculating the actual length of sticking zone, but by using recommended values from other studies.

Figure 3(*a*) shows the heat transfer model of the frictional heat source at the tool-chip interface on the chip side. The interface frictional heat source relative to the chip is a band heat source moving with velocity V_c. Considering the heat partition fraction for the chip $B(x)$, the heat liberation rate $B(x)q_{pl}(x)$ of the moving-band heat source is considered to be transferred into the chip. Since the chip thickness t_c is small, the boundary effect of the upper surface of the chip can be taken into account by adding an image heat source. The upper surface boundary of the chip is considered to be adiabatic. The temperature rise at any point

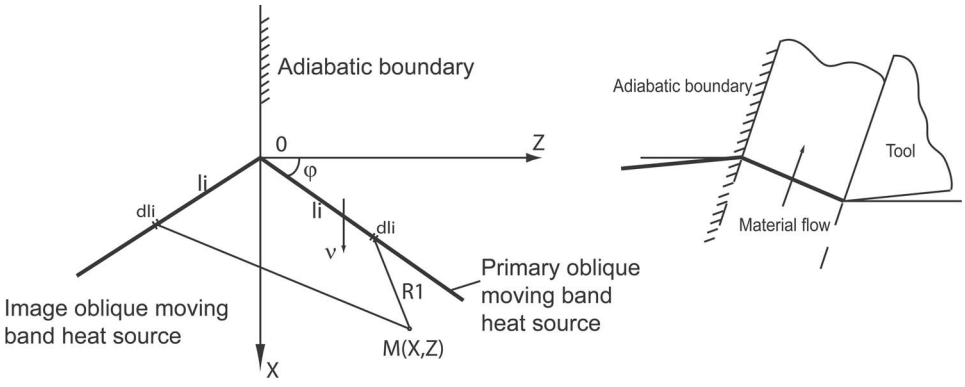

Fig. 2 Modified Hahn's model for an oblique band heat source in a semi-infinite medium

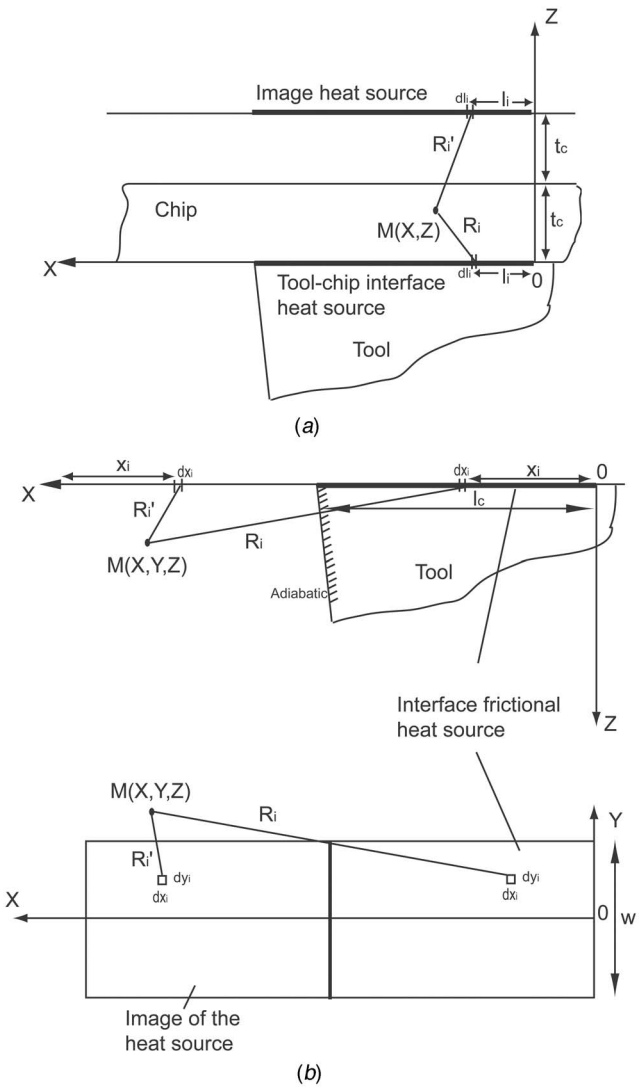

Fig. 3 Heat transfer model for the frictional heat source at the tool-chip interface (*a*) on the chip side as a moving band heat source (*b*) on the tool side as a stationary rectangular heat source

$M(X,Z)$ in the chip side is caused by the frictional moving heat source and its image heat source can be found as

$$T_{M_{\text{chip-friction}}}(X,Z) = \frac{1}{\pi\lambda_c}\int_{l_i=0}^{l_c} B(l_i)q_{pl}(l_i)e^{-(X-l_i)V_c/2a_c} \times \left[K_0\left(R_i\frac{V_c}{2a_c}\right) + K_0\left(R_i'\frac{V_c}{2a_c}\right)\right]dl_i \quad (5)$$

Figure 3(*b*) shows the heat transfer model of the frictional heat source at the tool-chip interface on the tool side. The interface frictional heat source relative to the tool is a stationary rectangular heat source. The tool clearance face is considered to be adiabatic. Considering the heat partition fraction for the chip $[1-B(x)]$, the heat liberation rate $[1-B(x)]\ q_{pl}(x)$ of the heat source is considered to be transferred into the tool. The temperature rise at any point $M(X,Y,Z)$ in the tool caused by the frictional stationary heat source including its image heat source, given as

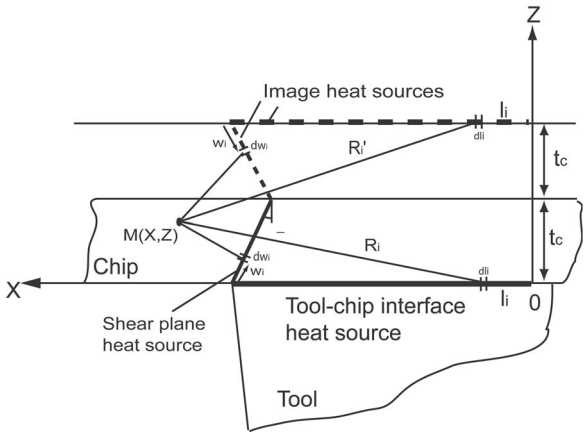

Fig. 4 Common coordinate system for combined effect heat sources

$$T_{M_{\text{tool-friction}}}(X,Z) = \frac{1}{2\pi\lambda_t}\int_{y_i=-w/2}^{w/2}\int_{x_i=0}^{l_c}[1-B(x_i)]q_{pl}(x_i) \times \left(\frac{1}{R_i}+\frac{1}{R_i'}\right)dx_i dy_i \quad (6)$$

In order to find the temperature rise in the tool caused by the shear plane heat source, heat coming from the shear plane heat source can be modeled as an induced stationary heat source located at the tool-chip interface. For the induced heat source, Eq. (6) can be used with some modifications where initially the heat intensity of the induced heat source is unknown but the average temperature rise caused by it at the tool-chip interface is known. The latter is obtained during the calculation of the temperature rise distribution in the chip at the tool-chip interface on the chip side as detailed in Eq. (5). Due to continuity of the heat flow, the temperature rise distribution at the tool-chip interface on the tool side is the same as that on the chip side. Therefore, the average heat liberation intensity of the induced heat source and heat partition ratios along tool-chip interface can be calculated. By using the information of average temperature equality at the interface, induced heat intensity of shear plane heat source can be calculated.

Using the above equations by considering $z=0$ and $y=0$, the local temperature rise at each point along the tool-chip interface can be calculated. Since the average temperature rise on both sides at the contacting interface should be the same, the distribution of the heat partition ratio can be calculated either numerically by satisfying Eq. (7) along every point on tool-chip interface or by assuming an expression for heat partition ratio and calculating the parameters of this expression by matching the temperature distribution curves on the tool and chip sides as in Komanduri and Hou [16].

$$T_{M_{\text{shear}}}(X,0) + T_{M_{\text{chip-friction}}}(X,0) = T_{M_{\text{tool-friction}}}(X,0,0) + T_{M_{\text{induced-shear}}}(X,0,0) \quad (7)$$

In order to ease application a common coordinate system should be chosen. The common coordinate system for the combined effect of primary and secondary heat sources is given in Fig. 4.

Nonlinear heat intensity of the secondary heat source, which is dependent on shear stress distribution on the tool-chip interface, will be calculated analytically. This approach is the refinement on the Komanduri and Hou [16] model in this study. Calculation of the shear stress distribution and the lengths of sticking and sliding zones, shown in Fig. 5, will be explained next.

Therefore, with the calculated heat partition ratios, the temperature rise at any point in the chip can be calculated with Eq. (8).

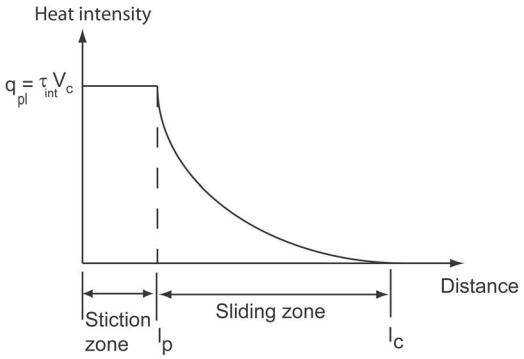

Fig. 5 Heat intensity model along the rake face of the tool

$$T_{M_{\text{chip}}}(X,Z) = T_{M_{\text{shear}}}(X,Z) + T_{M_{\text{chip-friction}}}(X,Z) + T_0 \tag{8}$$

The temperature rise at any given point in the tool can be calculated by

$$T_{M_{\text{tool}}}(X,0,Z) = T_{M_{\text{tool-friction}}}(X,0,Z) + T_{M_{\text{induced-shear}}}(X,0,Z) + T_0 \tag{9}$$

3 Analytical Modeling of the Cutting Process

A simplified illustration based on experimental observations of the plastic deformation for the formation of a continuous chip when machining a ductile material is given in Fig. 6. Oxley [4] assumed that the primary zone is a parallel-sided shear zone and the secondary deformation zone adjacent to the tool-chip interface is caused by the intense contact pressure and frictional force, which causes further plastic deformation.

Based on Oxley's model, the average value of the shear strain rate along AB is

$$\dot{\gamma}_{AB} = C_0 \frac{V_S}{l_{AB}} \tag{10}$$

The shear velocity V_s along the shear plane is

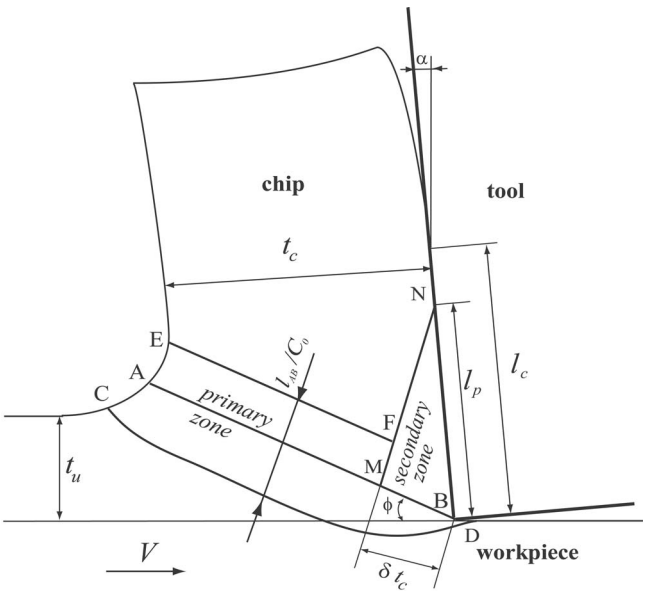

Fig. 6 Simplified deformation zones in orthogonal cutting

$$V_S = \frac{V\cos\alpha}{\cos(\phi-\alpha)} \tag{11}$$

Given by Eq. (12), l_{AB} is the length of primary zone AB, and can be calculated from geometry as

$$l_{AB} = \frac{t_u}{\sin(\phi)} \tag{12}$$

and C_0 is a constant representing the ratio of the thickness of the primary zone to the length of plane AB. Cut chip thickness can be estimated from Eq. (13) for a given shear angle ϕ as

$$t_c = \frac{t_u\cos(\phi-\alpha)}{\sin(\phi)} \tag{13}$$

and the strain in the middle of the primary shear zone is given as

$$\bar{\varepsilon}_{AB} = \frac{\cos\alpha}{2\sqrt{3}\sin\phi\cos(\phi-\alpha)} \tag{14}$$

In the primary zone, the flow stress on plane AB can be calculated by using Eq. (1) and the average value of shear stress at AB according to the Von Mises criterion can be calculated as

$$k_{AB} = \sigma_{AB}/\sqrt{3} \tag{15}$$

The shear force along AB may be calculated as

$$F_s = \frac{k_{AB}t_u w}{\sin\phi} \tag{16}$$

The hydrostatic pressures at A and B are

$$p_A = k_{AB}\left[1 + 2\left(\frac{\pi}{4} - \phi\right)\right] \tag{17}$$

$$p_B = k_{AB}\left(2\tan\theta - \left(1 + 2\left(\frac{\pi}{4} - \phi\right)\right)\right) \tag{18}$$

The angle between the resultant force and the direction of the primary shear zone θ can be obtained using the known pressure distribution and shear stress along the shear plane.

$$\theta = \tan^{-1}\left(1 + 2\cdot\left(\frac{\pi}{4} - \phi\right) - \frac{dk}{d\gamma}\frac{C_0\gamma_{AB}}{k_{AB}}\right) \tag{19}$$

where

$$\frac{dk}{d\gamma} = \frac{\partial k}{\partial\varepsilon}\frac{\partial\varepsilon}{\partial\gamma} + \frac{\partial k}{\partial T}\frac{\partial T}{\partial\gamma} + \frac{\partial k}{\partial\dot{\varepsilon}}\frac{\partial\dot{\varepsilon}}{\partial\gamma} \tag{20}$$

and after necessary differentiations

$$\frac{dk}{d\gamma} = \frac{1}{3}(Bn\varepsilon_{AB}^{n-1})\left(1 + C\ln\left(\frac{\dot{\varepsilon}_{AB}}{\dot{\varepsilon}_0}\right)\right)\left(1 - \left(\frac{T_{AB}-T_0}{T_m-T_0}\right)^m\right) + \frac{1}{\sqrt{3}}(A + B\varepsilon_{AB}^n)\left(1 + C\ln\left(\frac{\dot{\varepsilon}_{AB}}{\dot{\varepsilon}_0}\right)\right)\times\left(\frac{-m}{T_m-T_0}\left(\frac{T_{AB}-T_0}{T_m-T_0}\right)^{m-1}\right)\left(\frac{\partial T}{\partial\gamma}\right) \tag{21}$$

In Eq. (21) the derivation $\partial T/\partial\gamma$ should be computed numerically. The constant C_0 can be found by using the relation given in Eq. (22) [20]

$$C_0 = \frac{p_A - p_B}{k_u - k_l} \tag{22}$$

where k_u is the shear stress at upper boundary (EF in Fig. 6) and k_l shear stress at lower boundary (CD in Fig. 6) of the primary shear zone. In order to find k_u, strain at EF can be approximated by Eq. (23) and strain rate can be assumed to be constant all along the primary shear zone [20],

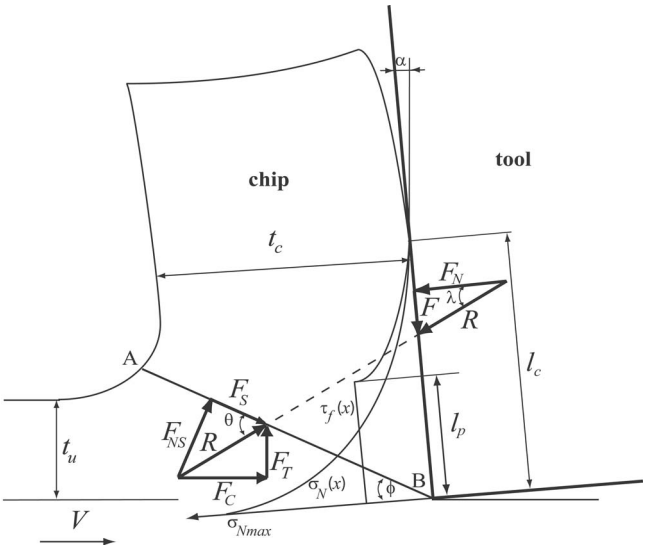

Fig. 7 Forces acting on the shear plane and the tool with resultant stress distributions on the tool rake face

$$\varepsilon_{EF} = 2\varepsilon_{AB} \tag{23}$$

and T_{EF} can be calculated analytically from its coordinates in the chip. Forces acting on the shear plane and the tool with assumed resultant stress distributions on the tool rake face are given in Fig. 7.

The distance between point B and the point where R cuts the shear the plane X_{sh} can be found by taking moments about the cutting edge of the normal stresses on the shear plane AB

$$X_{sh} = \frac{l_{AB}(2p_A + p_B)}{3(p_A + p_B)} \tag{24}$$

and the distance from the cutting edge to the point where the resultant force R intersects the tool cutting face X_{fr} can be found from geometry as given in Li [21]

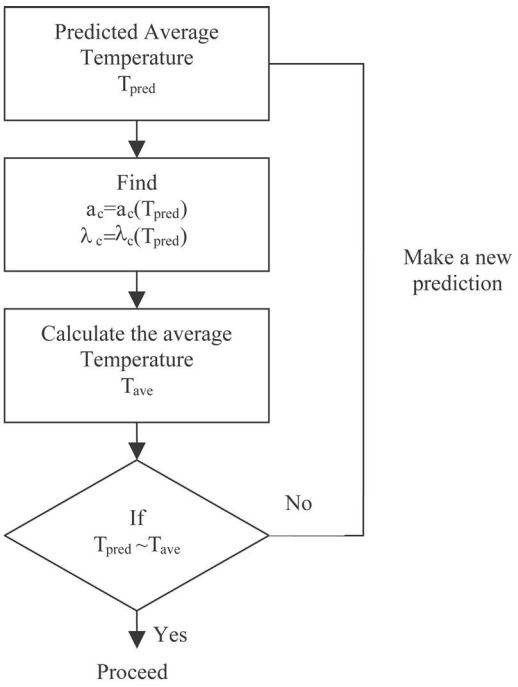

Fig. 8 Flow chart for computing average temperatures

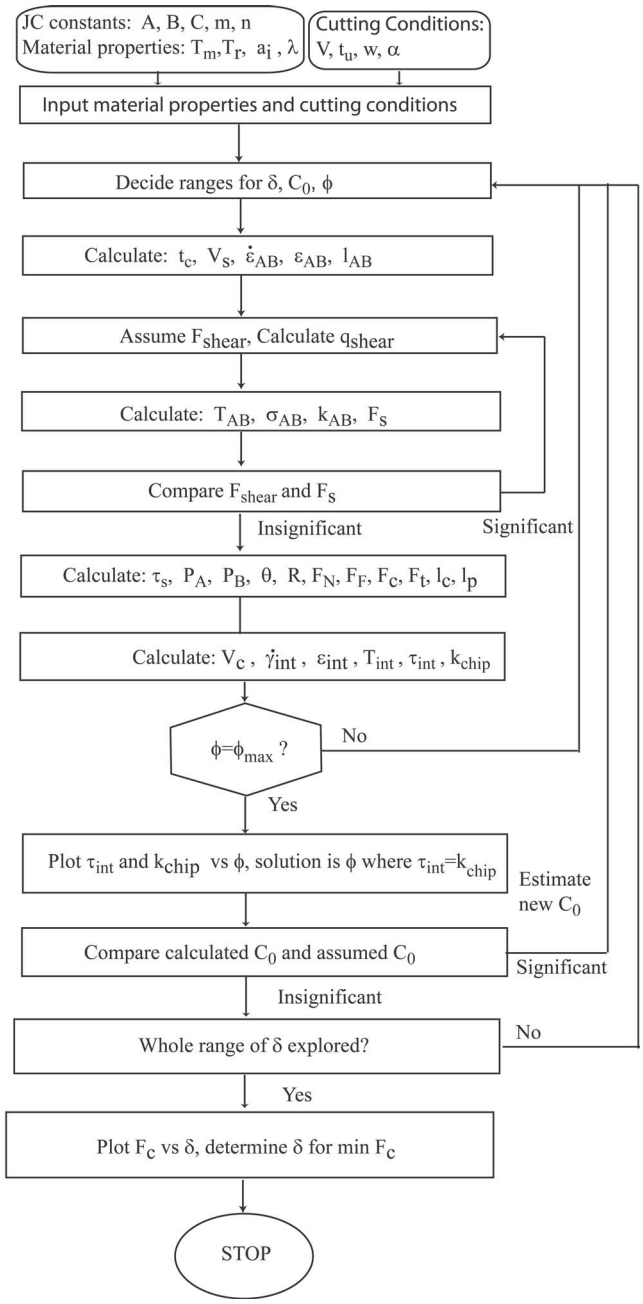

Fig. 9 Flow chart of the computational algorithm

$$X_{fr} = \frac{\sin\theta}{\sin\left(\frac{\pi}{2} + \phi - (\theta + \alpha)\right)} X_{sh} \tag{25}$$

The normal (F_N) and tangential (F) components of the resultant cutting force (R) on the tool rake face, cutting force F_c and thrust force F_t can be obtained

$$\begin{aligned} F_N &= R \cdot \cos(\theta - \phi + \alpha), \quad F = R \cdot \sin(\theta - \phi + \alpha) \\ F_c &= R \cdot \cos(\theta - \phi), \quad F_t = R \cdot \sin(\theta - \phi) \end{aligned} \tag{26}$$

Interfacial friction on the tool rake face is not continuous and is a function of the normal and frictional stress distributions. According to Zorev [3], the normal stress is greatest at the tool tip and gradually decreases to zero at the point where the chip separates from the rake face as shown in Fig. 7. The frictional shearing

Table 2 Cutting conditions for AISI 1045 steel (w=2) [24]

Test	V (m/min)	α (deg)	t_u (mm)	t_c (mm)[a]	ϕ (deg)[a]
1	200	−7	0.150	0.33	22
2	200	+5	0.150	0.33	25
3	200	−7	0.300	0.6	24
4	200	+5	0.300	0.6	27
5	300	−7	0.150	0.31	24
6	300	+5	0.150	0.31	26
7	300	−7	0.300	0.58	25
8	300	+5	0.300	0.56	29

[a]As predicted with the model.

stress distribution is more complicated. Over the portion of the tool-chip contact area near the cutting edge, sticking friction occurs, and the frictional shearing stress τ_{int} is equal to the average shear flow stress at tool-chip interface in the chip k_{chip}. Over the remainder of the tool-chip contact area, sliding friction occurs, and the frictional shearing stress can be calculated using the coefficient of friction μ_e. The normal stress distribution on the tool rake face can be described by

$$\sigma_N(x) = \sigma_{N_{\max}}\left[1 - \left(\frac{x}{l_c}\right)^a\right] \tag{27}$$

where $\sigma_{N_{\max}}$ is given by Oxley [4] as

$$\sigma_{N_{\max}} = p_B + 2k_{AB}(\phi - \alpha) \tag{28}$$

Unknowns in Eq. (27) are l_c and a, which require two equations to solve. Integrating the normal stress along the entire tool-chip contact length yields the relation in Eq. (29), which is equal to normal force on the tool rake face

$$F_N = \int_0^{l_c} w\sigma_N(x)dx = \int_0^{l_c} w\sigma_{N_{\max}}\left[1 - \left(\frac{x}{l_c}\right)^a\right]dx \tag{29}$$

Also taking the moment according to point B

$$F_N X_{fr} = \int_0^{l_c} w\sigma_N(x)xdx = \int_0^{l_c} w\sigma_{N_{\max}}\left[1 - \left(\frac{x}{l_c}\right)^a\right]xdx \tag{30}$$

and denoting

$$\mathbf{I} = \frac{\sigma_{N_{\max}} X_{fr} w}{F_N} \tag{31}$$

From Eqs. (29) and (30), the contact length along the tool-chip interface l_c and the exponent a can be obtained as

$$a = -1 + \frac{\sqrt{16\mathbf{I}^2 - 8\mathbf{I}}}{4\mathbf{I} - 2} \tag{32}$$

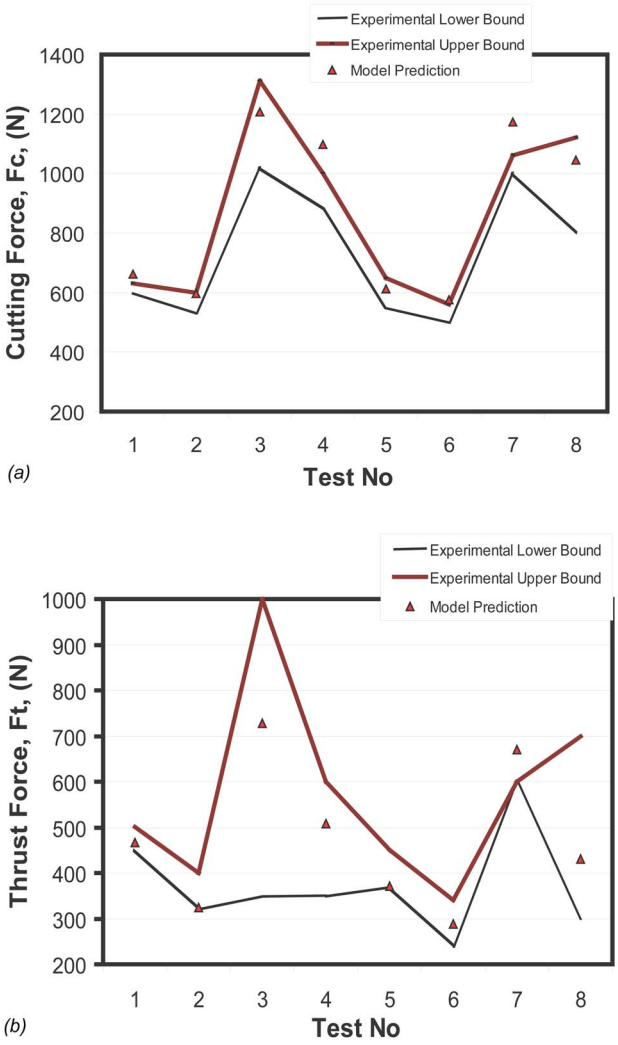

Fig. 10 Comparison of the predictions of the cutting force (*a*), and thrust force (*b*) with experimental data from [23]

$$l_c = \frac{F_N \cdot (a+1)}{aw\sigma_{N_{\max}}} \tag{33}$$

The shear stress distribution on the tool rake face illustrated in Fig. 7 can be represented in two distinct regions: (a) in the sticking region $\tau_{\text{int}}(x) = k_{\text{chip}}$ and when $\mu_e\sigma_N(x) \geq k_{\text{chip}}$, $0 < x \leq l_P$, (b) in the sliding region $\tau_{\text{int}}(x) = \mu_e\sigma_N(x)$ and when $\mu_e\sigma_N(x) < k_{\text{chip}}$, $l_P < x \leq l_c$. Here τ_{int} is the shear stress of the material at the tool-chip interface, and it is related to the frictional force between the chip and the tool, F_F, as

Table 3 Force and temperature predictions for AISI 1045 steel

Test	Predicted F_C (N)	Predicted F_T (N)	Predicted T_{AB}	Predicted max (T_{int})	Measured [23] max (T_{int})
1	662	466	370	1080	1120
2	596	324	332	1125	1250
3	1206	728	369	1170	1100
4	1097	509	319	1158	1220
5	613	371	370	1241	1310
6	576	288	330	1227	1300
7	1174	671	365	1329	1305
8	1046	430	311	1310	1300

Table 4 Predicted normal stress distribution parameters for machining AISI 1045 steel

Test	$\sigma_{N\max}$ (N/mm^2)	l_p (mm)	l_c (mm)	a
1	1380	0.12	0.6	0.75
2	992	0.11	0.54	1.1
3	1305	0.13	1.04	0.89
4	1007	0.28	0.91	1.3
5	1308	0.07	0.52	0.9
6	970	0.11	0.56	1.3
7	1325	0.14	0.98	0.91
8	1039	0.28	0.82	1.4

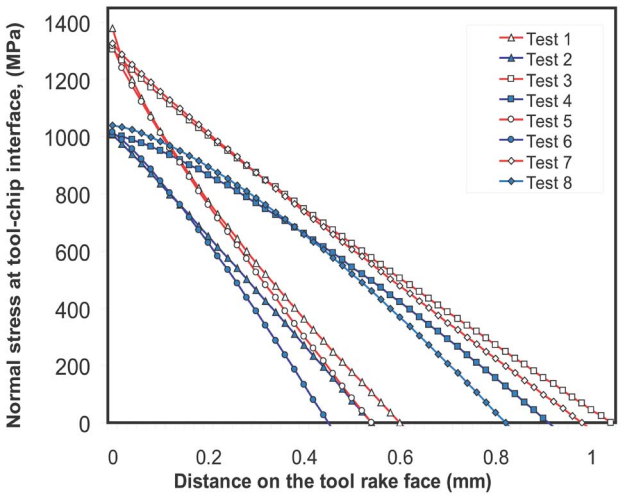

Fig. 11 Predicted stress distributions on the tool rake face for machining AISI 1045 steel

$$F_F = \int_0^{l_P} w\tau_{\text{int}} dx + \int_{l_P}^{l_C} w\mu_e \sigma_N(x) dx \tag{34}$$

The relation between the average coefficient of friction in the sliding region μ_e and τ_{int} is also given in

$$\mu_e = \frac{\tau_{\text{int}}}{\sigma_N(l_P)} \tag{35}$$

Combining Eqs. (36) and (37) leads to the expression for τ_{int} as shown in

$$\tau_{\text{int}} = \frac{F_F}{wl_P + \dfrac{w}{\sigma_N(l_P)} \displaystyle\int_{l_p}^{l_C} \sigma_N(x) dx} \tag{36}$$

The chip velocity can be calculated as

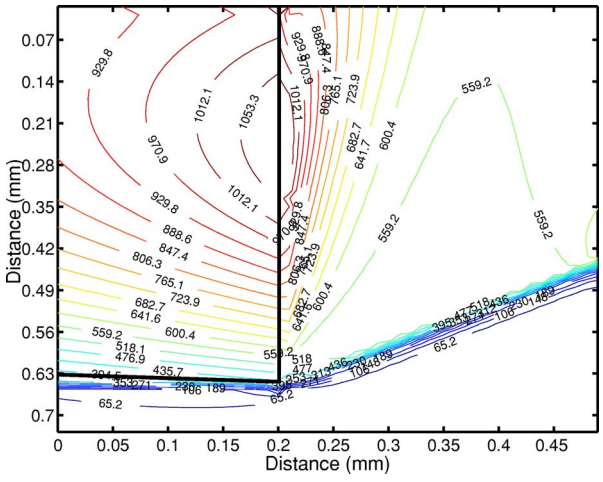

Fig. 12 Temperature distributions for AISI 1045 at conditions in test 1. (The figure is drawn perpendicular to the tool-chip interface for simplicity; the figure should be rotated 7 deg clockwise for actual view.)

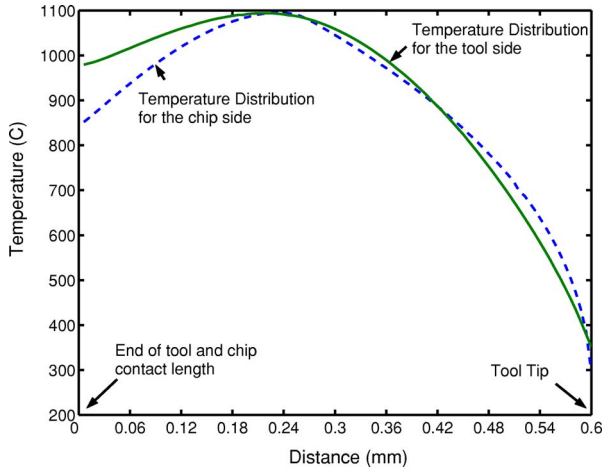

Fig. 13 Temperatures along the tool-chip interface for test condition 1 for AISI 1045

$$V_c = \frac{V \sin\phi}{\cos(\phi - \alpha)} \tag{37}$$

According to Oxley [4], the average shear strain rate and shear strain are considered constant and can be estimated from Eqs. (38) and (39) in the secondary zone.

$$\dot{\gamma}_{\text{int}} = \frac{V_c}{\delta \cdot t_c} \tag{38}$$

$$\gamma_{\text{int}} = \frac{l_P}{\delta \cdot t_c} \tag{39}$$

$$l_P = \frac{\delta \cdot t_c}{\sin(\phi - \alpha)} \tag{40}$$

The flow stress at tool chip interface k_{chip} can be found by utilizing Eq. (1)

$$k_{\text{chip}} = \frac{1}{\sqrt{3}}[A + B(\bar{\varepsilon})^n]\left[1 + C\ln\left(\frac{\dot{\bar{\varepsilon}}}{\dot{\bar{\varepsilon}}_0}\right)\right]\left[1 - \left(\frac{T_{\text{int}_{\text{stiction}}} - T_0}{T_m - T_0}\right)^m\right] \tag{41}$$

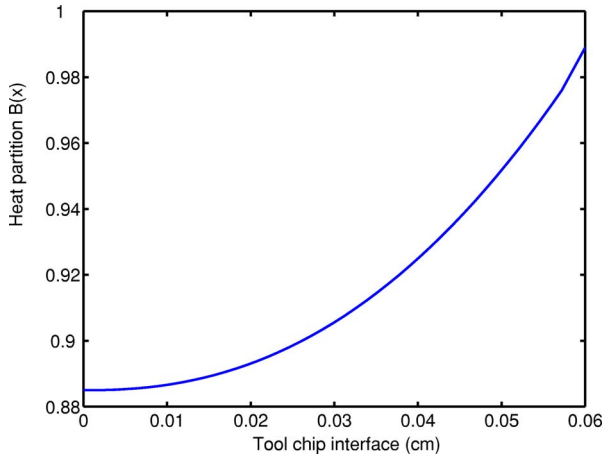

Fig. 14 Heat partition ratio along the tool chip interface for test condition 1 for AISI 1045

Table 5 Cutting conditions and predictions of force and temperatures for machining Al6082-T6 (α=8 deg, w=3 mm)

			Predicted						Measured [20]		
Test	V (m/min)	t_u (mm)	t_c (mm)	ϕ (deg)	F_C (N)	F_T (N)	T_{AB} (°C)	T_{int} (°C)	T_{AB} (°C)	F_C (N)	F_T (N)
1	120	0.2	0.52	21.7	550	405	217	498	210	552	384
2	240	0.4	0.76	29.2	767	273	221	464	205	795	300
3	360	0.2	0.44	25.2	443	221	228	493	188	456	204
4	360	0.4	0.64	33.8	719	223	214	508	198	768	276

4 Solution of the Combined Thermal and Analytical Modeling of the Cutting Process

For the proposed orthogonal machining model, cutting conditions, and the material properties of the workpiece are the inputs. The outputs are process related variables, such as shear angle, contact length, cutting forces, tool stress distributions, and temperature distribution in the chip and along the tool-chip interface. The shear angle, strain rate constant, and the ratio of thickness of the tool-chip interface plastic zone to chip thickness are selected based on the minimum force principle. As discussed above, the temperature rise along shear zone (X,Z) can be calculated as given in Eq. (3). The average temperature in primary shear zone can be found by integrating Eq. (3) along the shear length, given as

$$T_{AB} = \frac{\int_0^{l_{AB}} T_{M_{\text{shear}}}(X,Z)dl_i}{l_{AB}} + T_0 \tag{42}$$

The heat partition ratio expression $B(X)$ is adopted from Komanduri and Hou [16] and given in

$$B(x) = (B_{\text{chip}} - \Delta B_1) + 2\Delta B_1\left(\frac{x}{l_c}\right)^{m_1}$$
$$1 - B(x) = (B_{\text{tool}} + \Delta B_1) - 2\Delta B_1\left(\frac{x}{l_c}\right)^{m_1} \tag{43}$$

In this expression, the coefficients B_{chip}, ΔB_1, and m_i should be calculated by matching the temperature distribution curves as much as possible along the tool-chip interface. The discussions about this expression are given in Komanduri and Hou [16]. Once the $B(x)$ expression is calculated, the average temperature on the tool chip interface can be found as

$$T_{\text{int}} = \frac{\int_0^{l_c} T_{M_{\text{shear}}}(X,0) + T_{M_{\text{chip-friction}}}(X,0,0)dl_i}{l_c} + T_0 \tag{44}$$

The thermal conductivity (λ_c) and thermal diffusivity (a_c) coefficients of the workpiece are considered to be constant in the thermal model, but in fact they depend on temperature. An iterative approach is used in calculation of the temperatures. For example, an average temperature for the primary shear zone is predicted, thermal conductivity and diffusivity at that predicted average temperature are found and actual average temperature is calculated by using these constants. The iteration continues until the predicted and average temperature calculations are close, as shown in the flow chart given in Fig. 8. Thermal conductivity of the carbide tool is taken constant as 0.4 J/cm s°C.

The shear angle ϕ is determined according to the fact that the tool-chip interface shear stress τ_{int} caused by the resultant cutting force for a given set of cutting conditions must be equal to the chip material flow stress k_{chip} at the sticking region, which is the function of strain, strain rate, and temperature at the interface for the same cutting condition. Since heat intensity is required to obtain temperature distribution in the primary shear zone, shear force is found through trial and error until assumed and calculated shear forces are identical. The search for the true value of ϕ will go through iterations until the calculated interface shear stress and the material shear flow stress are equal. If there is more than one shear angle that satisfies the above condition, the highest angle is chosen. Reasonable values of C_0 and δ are also searched iteratively at the same time to simultaneously satisfy the conditions. The flow chart of this approach is summarized in Fig. 9.

Table 6 Other predictions for Al6082-T6 (α=8 deg, w=3 mm)

Test	$\sigma_{N\max}$ (N/mm^2)	l_p (mm)	l_c (mm)	a
1	420.8	0.35	1.1	0.542
2	322.3	0.45	0.935	1.11
3	315.2	0.31	0.67	1.76
4	436	0.23	0.92	1.28

5 Model Validation and Results

In order to validate the predictive thermal and analytical modeling approach for metal cutting processes presented in this paper, a set of orthogonal cutting experiments for machining AISI 1045 steel [23], AL 6082-T6 aluminum alloy [20,24], and AL6061-T6 aluminum alloy [20] is utilized. Experimental data include measured cutting and thrust forces and average temperatures on the shear plane and at the tool-chip interface.

5.1 Model Validation for Steel Machining. The cutting conditions for machining AISI 1045 are given in Table 2. In these cutting conditions, machining with both a negative (−7 deg) and a

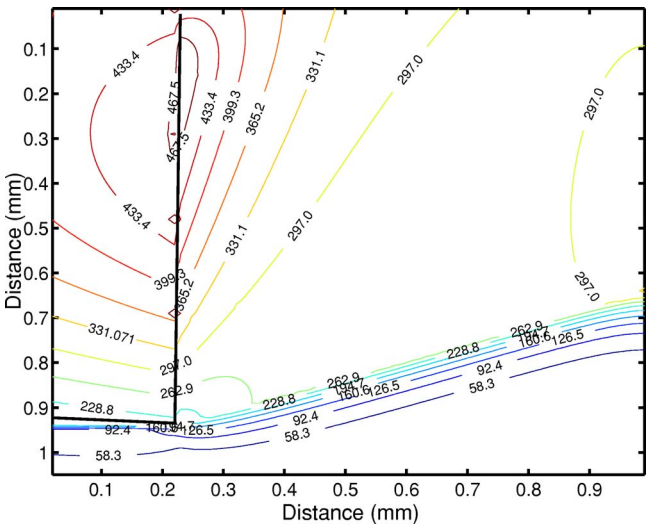

Fig. 15 Temperature distributions in the chip for Al 6082-T6 at conditions in test 2

Table 7 Cutting conditions and predictions of force and temperatures for machining Al6061-T6 (α=8 deg, w=3.3 mm)

			Predicted						Measured [20]		
Test	V (m/min)	t_u (mm)	t_c (mm)	ϕ (deg)	F_C (N)	F_T (N)	T_{AB} (°C)	T_{int} (°C)	t_c (mm)	F_C (N)	F_T (N)
1	165	0.16	0.44	20.6	470	383	184	443	0.45	475	388
2	225	0.16	0.41	22	430	311	190	453	0.4	450	315
3	165	0.32	0.8	22.6	821	572	199	485	0.7	825	545
4	225	0.32	0.75	24	762	475	202	503	0.78	785	415

Table 8 Other predictions for Al6061-T6 (α=8 deg, w=3.3 mm)

Test	$\sigma_{N\max}$ (N/mm^2)	l_p (mm)	l_c (mm)	a
1	412.6	0.5	1.0	0.43
2	378.3	0.42	0.85	0.55
3	366	0.82	1.62	0.6
4	348	0.7	1.4	0.73

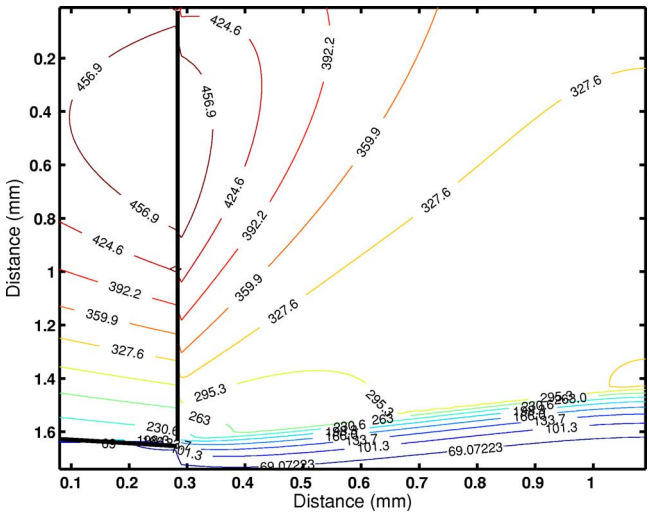

Fig. 16 Temperature distributions in the chip for Al 6061-T6 at conditions in test 3

positive rake (5 deg) angle were tested. Chip thickness and shear angle were calculated as presented in Table 2. The predicted temperatures are compared with experimental values in Table 3. The predicted forces are compared with the experiments for machining AISI 1045 steel as shown in Fig. 10. The comparison with the measured forces shows that the force predictions are in close agreement. The measured temperatures and the predicted temperatures at the tool-chip interface in machining of AISI 1045 steel indicate agreements for Tests 1, 2, and 4. However, more refined measurements of temperature distributions during the cutting process are needed to validate predicted temperature distributions and heat partitions. Such measurements for machining of AISI 1045 steel were performed by Davies et al. [25]. Figure 10 shows the cutting and thrust force predictions of the proposed model under AMM test [23] conditions. For the cases presented, the predicted forces are in good agreement with the experimental values and always remain within upper and lower limits [27,28].

In addition, the predictions for normal stress distribution on the tool rake face for machining AISI 1045 steel are given in Table 4 and Fig. 11. The predicted normal stress distributions depict that the power law exponent a is less than 1 for machining at negative rake angles and greater than 1 for machining at positive rake angles. This behavior affects temperature predictions since nonuniform heat partition at the tool-chip interface is obtained from normal stress distributions on the tool rake face.

The temperature distributions in the tool, chip, and workpiece can be obtained by dividing the tool, chip, and workpiece into small increments and calculating the temperature rise at every point. Figure 12 shows the temperature distributions in the chip, tool and workpiece.

The nonuniform heat partition distribution at the tool-chip interface is given in Fig. 13 and variation of heat partition ratio is shown in Fig. 14. When uniform heat intensity is used in thermal modeling maximum temperature is obtained close to the end of the tool-chip interface. Due to nonlinear heat intensity modeling, where the length of the sticking zone is considered, the location of maximum temperature gets closer to the middle of the tool chip interface. The temperature rise distribution along the tool-chip interface for chip and tool side is shown in Fig. 13. The discrepancy between temperature rise curves can be reduced by using a heat partition expression, which has higher power terms.

5.2 Model Validation for Aluminum Machining. The cutting conditions for machining AL6082-T6 that are adapted from Adibi-Sedeh et al. [20] and Jaspers and Dautzenberg [24] are given in Table 5. The predicted forces, temperatures and parameters of normal stress distributions are presented in Tables 5 and 6 for machining AL6082-T6. The temperature distributions in the chip, tool, and workpiece for AL-6082-T6 (test 2) are given in Fig. 15.

The model validation is also performed on machining AL6061-T6 aluminum alloy. The cutting conditions for machining AL6061-T6 that are adapted from Adibi-Sedeh et al. [20] are given in Table 7. The predicted forces, temperatures, and parameters of normal stress distributions are presented in Tables 7 and 8 for machining AL6082-T6. The temperature distributions in the chip, tool and workpiece for AL-6082-T6 (test 3) are given in Fig. 16.

6 Conclusion

This paper combines oblique moving band heat source theory with nonuniform heat intensity at tool-chip interface and modified Oxley's parallel shear zone theory to predict cutting forces, stress, and temperature distributions. The proposed methodology has been applied to two different materials, and promising results in close agreement with experimental results have been obtained. As a major contribution, the methodology proposed here predicts detailed temperature distributions for machining of AISI 1045 steel, AL-6082-T6, and AL 6061-T6, aluminum alloys as shown in Figs. 12, 15, and 16. The model provides significant advantages from the tool wear modeling point of view.

Acknowledgment

This research is supported by the Rutgers University Research Council Grants program under the Grant No. 2-02321.

Nomenclature

A = plastic equivalent strain in Johnson-Cook constitutive model (MPa)
a = power exponent of the normal stress distribution on the tool rake face
a_i = thermal diffusivity of the medium i
B = strain related constant in Johnson-Cook constitutive model (MPa)
$B(x)$ = heat partition fraction
C = strain-rate sensitivity constant in Johnson-Cook constitutive model
C_0 = strain rate constant proposed by Oxley
F_C, F_T = cutting and thrust force components (N)
F_F, F_N = frictional and normal force components at tool rake face (N)
F_S, F_{NS} = shear force and normal to the shear force components at AB (N)
K_0 = zero order Bessel function of the second kind
k_{AB} = shear flow stress on AB (N/mm^2)
k_{chip} = shear flow stress in chip at tool-chip interface (N/mm^2)
l_{AB} = length of the primary shear zone (mm)
l_c = length of tool-chip contact (mm)
l_p = length of sticking region (mm)
m = thermal softening parameter in Johnson-Cook constitutive model
n = strain-hardening parameter in Johnson-Cook constitutive model
p_A, p_B, p_M, p_N = hydrostatic stresses at the points A, B, M, and N (N/mm^2)
q = heat intensity
T_0 = initial work material temperature (°C)
T_{AB} = average temperature along AB (°C)
T_{int} = average temperature along tool-chip interface (°C)
T_m = melting temperature of the work material (°C)
t_u, t_c = undeformed and deformed chip thickness (mm)
V, V_S, V_C = cutting velocity, shear velocity, and chip velocity (m/sec)
w = width of cut (mm)
α = tool rake angle (degree)
δ = proportion of the thickness of the secondary zone to the chip thickness
$\bar{\varepsilon}_{AB}, \bar{\varepsilon}_{\text{int}}$ = effective strain at AB and tool-chip interface (mm/mm)
$\dot{\bar{\varepsilon}}_0$ = reference strain rate (s^{-1})
$\dot{\bar{\varepsilon}}_{AB}, \dot{\bar{\varepsilon}}_{\text{int}}$ = effective strain rate at AB and tool-chip interface (s^{-1})
ϕ = shear angle (deg)
$\bar{\gamma}_{AB}, \bar{\gamma}_{\text{int}}$ = effective shear strain at AB and tool-chip interface (mm/mm)
$\dot{\bar{\gamma}}_{AB}, \dot{\bar{\gamma}}_{\text{int}}$ = effective shear strain-rate at AB and tool-chip interface (s^{-1})
μ_e = coefficient of friction in the elastic contact region of tool-chip interface
ρ = density (kg/m^3)
$\bar{\sigma}_{AB}$ = effective flow stress at AB (N/mm^2)
σ_N = normal stresses acting on tool-chip interface (N/mm^2)
τ_{int} = frictional shear stress at tool-chip interface (N/mm^2)
λ = thermal conductivity (W/m°C)

References

[1] Ernst, H., and Merchant, M. E., 1941, "Chip Formation, Friction and High Quality Machined Surfaces," Trans. Am. Soc. Met., **29**, pp. 299–378.
[2] Lee, E. H., and Shaffer, B. W., 1951, "The Theory of Plasticity Applied to a Problem of Machining," J. Appl. Mech., **18**, pp. 405–413.
[3] Zorev, N. N., 1963, "Inter-Relationship Between Shear Processes Occurring Along Tool Face and Shear Plane in Metal Cutting," *International Research in Production Engineering ASME*, New York, pp. 42–49.
[4] Oxley, P. L. B., 1989, *Mechanics of Machining, an Analytical Approach to Assessing Machinability*, Ellis Horwood Limited, Chichester, England.
[5] Childs, T. H. C., 1998, "Material Property Needs in Modeling Metal Machining," *Proceedings of the CIRP International Workshop on Modeling of Machining Operations*, Atlanta, Georgia, I. S. Jawahir, A. K. Balaji, and R. Stevenson, eds., University of Kentucky Publishing Services, Lexington, KY, May 19, pp. 193–202.
[6] Özel, T., and Altan, T., 2000, "Determination of Workpiece Flow Stress and Friction at the Chip-Tool Contact for High-Speed Cutting," Int. J. Mach. Tools Manuf., **40**(1), pp. 133–152.
[7] Özel, T., and Zeren, E., 2005, "A Methodology to Determine Work Material Flow Stress and Tool-Chip Interfacial Friction Properties by Using Analysis of Machining," ASME J. Manuf. Sci. Eng., in press.
[8] Johnson, G. R., and Cook, W. H., 1983, "A Constitutive Model and Data for Metals Subjected to Large Strains, High Strain Rates and High Temperatures," *Proceedings of the 7th International Symposium on Ballistics*, The Hague, The Netherlands, April 21–26, pp. 541–547.
[9] Hahn, R. S., 1951, "On the Temperature Developed at the Shear Plane in the Metal Cutting Process," *Proceedings of First US National Congress of Applied Mechanics*, pp. 661–666.
[10] Trigger, K. J., and Chao, B. T., 1951, "An Analytical Evaluation of Metal Cutting Temperatures," Trans. ASME, **73**, pp. 57–68.
[11] Chao, B. T., and Trigger, K. J., 1953, "The Significance of the Thermal Number in Metal Machining," Trans. ASME, **75**, pp. 109–120.
[12] Leowen, E. G., and Shaw, M. C., 1954, "On the Analysis of Cutting Tool Temperatures," Trans. ASME, **71**, pp. 217–231.
[13] Leone, W. C., 1954, "Distribution of Shear Zone Heat in Metal Cutting," Trans. ASME, **76**, pp. 121–125.
[14] Boothroyd, G., 1963, "Temperatures in Orthogonal Metal Cutting," Proc. Inst. Mech. Eng., **177**, pp. 789–810.
[15] Komanduri, R., and Hou, Z. B., 2001, "Thermal Modeling of the Metal Cutting Process, Part 1: Temperature Rise Distribution Due to Shear Plane Heat Source," Int. J. Mech. Sci., **42**, pp. 1715–1752.
[16] Komanduri, R., and Hou, Z. B., 2001, "Thermal Modeling of the Metal Cutting Process, Part 2: Temperature Rise Distribution Due to Frictional Heat Source at the Tool-Chip Interface," Int. J. Mech. Sci., **43**, pp. 57–88.
[17] Komanduri, R., and Hou, Z. B., 2001, "Thermal Modeling of the Metal Cutting Process, Part 3: Temperature Rise Distribution Due to Combined Effects of Shear Plane Heat Source and the Tool-Chip Interface Frictional Heat Source," Int. J. Mech. Sci., **43**, pp. 89–107.
[18] Huang, Y., and Liang, S. Y., 2003, "Modelling of the Cutting Temperature Distribution Under the Tool Flank Wear Effect," Proc. Inst. Mech. Eng., Part C: J. Mech. Eng. Sci., **217**, pp. 1195–1208.
[19] Jaspers, S. P. F. C., and Dautzenberg, J. H., 2002, "Material Behavior in Conditions Similar to Metal Cutting: Flow Stress in the Primary Shear Zone," J. Mater. Process. Technol., **122**, pp. 322–330.
[20] Adibi-Sedeh, A. H., Madhavan, V., and Bahr, B., 2003, "Extension of Oxley's Analysis of Machining to Use Different Material Models," ASME J. Manuf. Sci. Eng., **125**, pp. 656–666.
[21] Johnson, G. R., Stryk, R. A., Holmquist, T. J., and Beissel, S. R., 1996, *User Instruction for the 1996 Version of the EPIC Code*, Alliant Techsystems Inc.
[22] Jaeger, J. C., 1942, "Moving Sources of Heat and the Temperatures at Sliding Contacts," J. Proc. R. Soc. N. S. W., **76**, pp. 203–224.
[23] Ivester, R. W., Kennedy, M., Davies, M., Stevenson, R., Thiele, J., Furness, R., and Athavale, S., 2000, "Assessment of Machining Models: Progress Report," Mach. Sci. Technol., **4**(3), pp. 511–538.
[24] Jaspers, S. P. F. C., and Dautzenberg, J. H., 2002, "Material Behavior in Metal Cutting: Strains, Strain Rates and Temperatures in Chip Formation," J. Mater. Process. Technol., **121**, pp. 123–135.
[25] Davies, M. A., Cao, Q., Cooke, A. L., and Ivester, R., 2003, "On the Measurement and Prediction of Temperature Fields in Machining 1045 Steel," CIRP Ann., **52**(1), pp. 77–80.
[26] Li, X., 1997, "Development of a Predictive Model for Stress Distributions at the Tool-Chip Interface In Machining," J. Mater. Process. Technol., **63**, pp. 169–174.
[27] Tay, A. O., Stevenson, M. G., and de Vahl Davis, G., 1974, "Using the Finite Element Method to Determine Temperature Distributions in Orthogonal Machining," *Proceedings of Institution for Mechanical Engineers*, **188**, pp. 627–638.
[28] Adibi-Sedeh, A. H., and Madhavan, V., 2002, "Effect of Some Modifications to Oxley's Machining Theory and the Applicability of Different Material Models," Mach. Sci. Technol., **6**(3), pp. 379–395.